Supporting information

Room temperature-formed iron-doped nickel hydroxide on nickel foam as 3D electrode for low polarized and high-current-density oxygen evolution

Chun Xian Guo*[a], Chang Ming Li*[a,b]

[a]Institute of Materials Science and Devices, Suzhou University of Science and Technology, Suzhou, 215003, P.R. China.

[b]Institute for Clean Energy & Advanced Materials, Southwest University, Chongqing 400715, P.R. China.

*E-mail: cxguo@usts.edu.cn; ecmli@swu.edu.cn

Part 1: Experimental methods

Fabrication of electrodes. Before electrode fabrication, Ni foam (thickness of 1.6 mm and bulk density of 0.45 g cm^{-3}) was cleared by ethanol and water, and then dried at room temperature. Room temperature-formed iron-doped nickel hydroxide (RT-Fe@$Ni(OH)_2$) on Ni foam was fabricated by immersing the as-cleaned Ni foam into commonly used Ni etching solution that contains $FeCl_3$ and HCl (1M/1M).[S1,S2] It is found that the immersion time of 5 mins treatment is the optimized one to achieve the best OER performance for the RT-Fe@$Ni(OH)_2$ electrode. Then the etched Ni foam was taken out of the etching solution, washed with water and dried at room temperature. Fe content in the electrode was adjusted by changing $FeCl_3$ concentration in the etching solution, achieving an atomic percentage ranging from 0 to 9.4%. A control electrode of RT-$Ni(OH)_2$ electrode was also fabricated using similar procedure as that of the RT-Fe@$Ni(OH)_2$ electrode but without $FeCl_3$ in the etching solution. A 3D electrode of iron-doped nickel hydroxide on Ni foam was fabricated with dip-coating and 300 ^oC treatment (Fe@$Ni(OH)_2$-300^oC),[S3] and the other electrode of Fe doped Ni LDH on Ni foam was hydrothermally synthesized (FeNi-LDH).[S4] Iridium nanoparticles (Ir NPs) were synthesized from $IrCl_3$ using a hydrothermal method with procedure as followings. 220 mg Nafion (5 wt%) and 0.5 ml H_2IrCl_6 solutions were added into a solution containing 5 ml water and 7.5 ml ethanol with magnetic stirring under N_2 atmosphere. As 1.4 ml of 1 M NaOH aqueous solution was added, the color of the solution turned to light green after 30 min. The mixture was transferred into an autoclave, then heated up to 125 °C for 5 h. After

cooling to room temperature, the obtained colloid solution was treated by dialysis to remove impurity ions and organic by products. Ir NPs electrode was prepared by coating Ir NPs on Ni foam with a loading amount of around 0.1 mg cm^{-2}.

Material characterizations. Field emission scanning electron microscopy (FESEM) was performed by JEOL JSM-6700F at 10 kV. Transmission electron microscopic (TEM) images were recorded by a JEOL JEM-2010F microscope at 200 kV. Elemental distribution was investigated by energy dispersive X-ray spectroscopy (EDS) from Oxford/INCA EDS. X-ray diffraction (XRD) patterns were measured using X-ray diffractometer (GADDS XRD system, Bruker AXS) with a CuKα source (λ=1.54 Å). X-ray photoelectron spectroscopy (XPS) characterizations were performed on a PHI Quantera x-ray photoelectron spectrometer with an Al cathode as the X-ray source.

Electrochemical testing. All electrochemical characterizations were measured using electrochemical workstation Chi760E at room temperature (25 ^{o}C). As-prepared electrodes were used as the working electrode without further treatment, and saturated calomel electrode (SCE) was used as the reference electrode. All potentials measured were calibrated to RHE using the following equation: $E_{RHE} = E_{SCE} + 0.241\ V + 0.059 \times pH$. For the pH of 1 M KOH aqueous solution, its pH was measured to be 13.8 at room temperature. For the 30wt% KOH aqueous solution (around 6.87 mol/L), its pH value is difficult to be measured using pH meter, and the value was estimated to be pH = 14 – (–log6.87) = 14.84. Tafel slope of the electrodes was derived from polarization curves with iR compensation. Chronoampermetric and chronopotentiometric measurements were obtained without iR compensation.

Calculation of turnover frequency (TOF). Assuming Ni species is the active site, TOF values were calculated according to the equation of TOF = $j \times A/(4 \times F \times m)$,[S5] where j (A cm^{-2}) is the current density obtained at a specific applied potential, A (cm^2) is the area of the electrode, F is the Faraday efficiency and m is the number of moles of Ni on surface of the electrode. m was estimated by measuring specific surface area of the electrode by N_2 adsorption/desorption isotherms, and then calculating the number of the Ni atoms at the surface using a value of 6.4×10^{18} Ni atoms per m^2 as reported,[S6] assuming all the surface atoms are Ni.

References

S1. K. S. Kim, Y. Zhao, H. Jang, S. Y. Lee, J. M. Kim, K. S. Kim, J.-H. Ahn, P. Kim, J.-Y. Choi and B. H. Hong, *Nature*, 2009, **457**, 706-710.

S2. Z. Chen, W. Ren, L. Gao, B. Liu, S. Pei and H.-M. Cheng, *Nat. Mater.*, 2011, **10**, 424-428.

S3. G. F. Dong, M. Fang, J. S. Zhang, R. J. Wei, L. Shu, X. G. Liang, S. P. Yip, F. Y. Wang, L. H. Guan, Z. J. Zheng and J. C. Ho, *J. Mater. Chem. A*, 2017, **5**, 11009-11015.

S4. Y. Lu, B. Jiang, L. Fang, F. L. Ling, F. Wu, B. S. Hu, F. M. Meng, K. Y. Niu, F. Lin and H. M. Zheng, *J Alloys Compd.*, 2017, **714**, 63-70.

S5. N. Jiang, B. You, M. Sheng and Y. Sun, *Angew. Chem. Int. Ed.*, 2015, **54**, 6251-6254.

S6. M. W. Louie and A. T. Bell, *J. Am. Chem. Soc.*, 2013, **135**, 12329-12337.

S7. T. Tang, W.-J. Jiang, S. Niu, N. Liu, H. Luo, Y.-Y. Chen, S.-F. Jin, F. Gao, L.-J. Wan and J.-S. Hu, *J. Am. Chem. Soc.*, 2017, **139**, 8320-8328.

S8. L. Yang, Z. Guo, J. Huang, Y. Xi, R. Gao, G. Su, W. Wang, L. Cao and B. Dong, *Adv. Mater.*, 2017, doi:10.1002/adma.201704574.

S9. X. Long, S. Xiao, Z. Wang, X. Zheng and S. Yang, *Chem. Commun.*, 2015, **51**, 1120-1123.

S10. J. Y. Zhang, L. Lv, Y. Tian, Z. Li, X. Ao, Y. Lan, J. Jiang and C. Wang, *ACS Appl. Mater. Interfaces*, 2017, **9**, 33833-33840.

Part 2: Additional table

Table S1. OER performance comparison of the RT-Fe@$Ni(OH)_2$ electrode with some recently reported 3D electrodes on Ni foam in 1 M KOH alkaline electrolyte.

Electrode	**Electrolyte**	***η* (V) at 100 mA cm^{-2}**	***k* (mV dec^{-1})**	**Ref**
RT-Fe@$Ni(OH)_2$ on Ni foam	1 M KOH	0.312	44.2	This work
3D Co-Mn carbonate hydroxide on Ni foam	1 M KOH	0.349	N/A	Ref.[S7]
3D Co-Mn carbonate hydroxide on Ni	1 M KOH	0.462 (1000 mA cm^{-2})	N/A	Ref.[S7]

foam				
3D $FePO_4$ on Ni Foam	1 M KOH	0.490	42.7	Ref.[S8]
3D CoNiFe hydroxide on Ni foam	1 M KOH	~0.25 (40 mA cm^{-2})	42	Ref.[S9]
3D $Co_{0.4}Fe_{0.6}Se_2$ on Ni foam	1 M KOH	~0.37	41	Ref.[S10]

Part 3: Additional figures

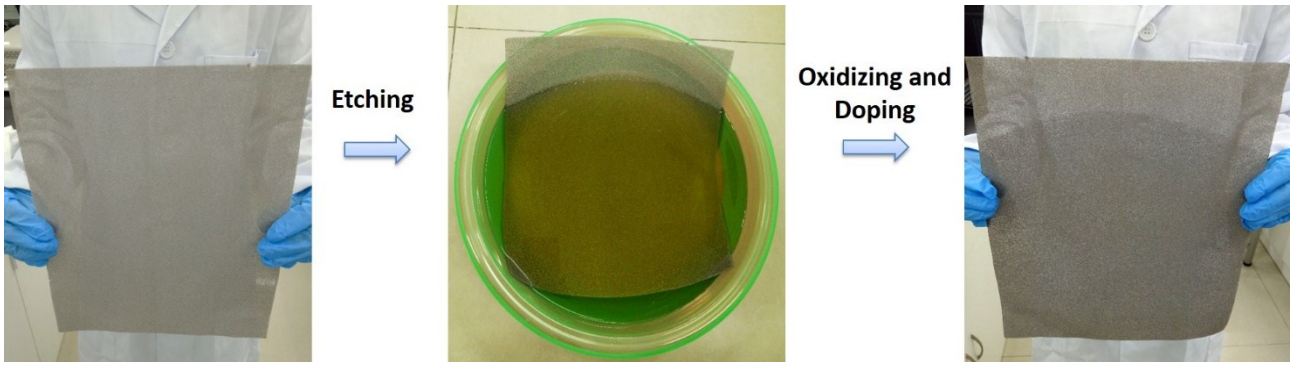

Fig. S1. Photograph showing the use of room temperature-based surficial etching and doping method for large-scale fabrication of the 3D electrode. Size of the foam is around 0.30 m × 0.35 m.

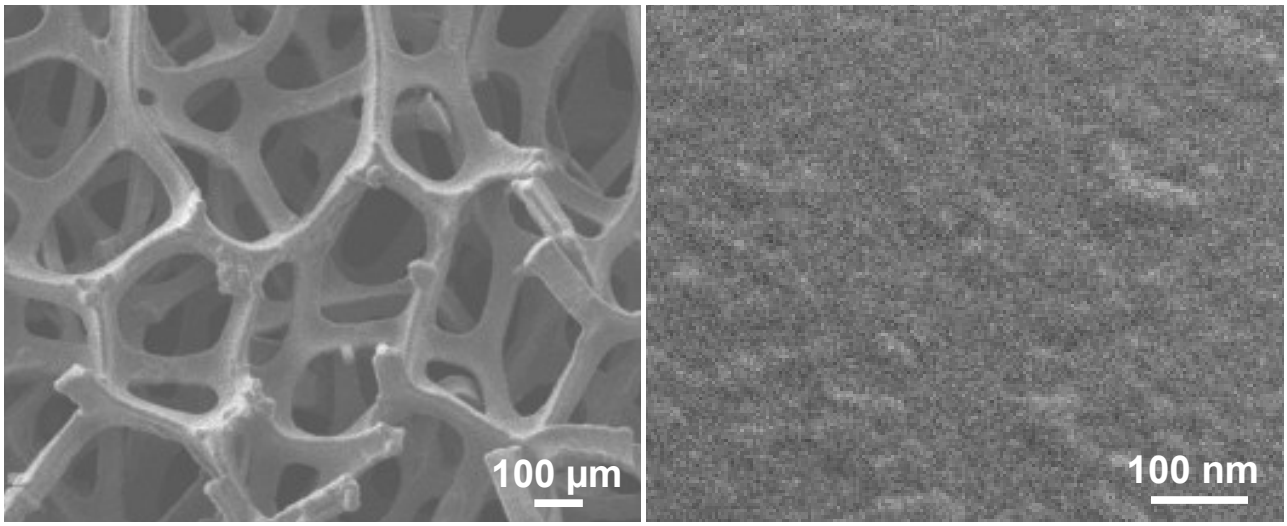

Fig. S2. SEM images of Ni foam before the room temperature-based surficial etching and doping process, showing a smooth surface structure.

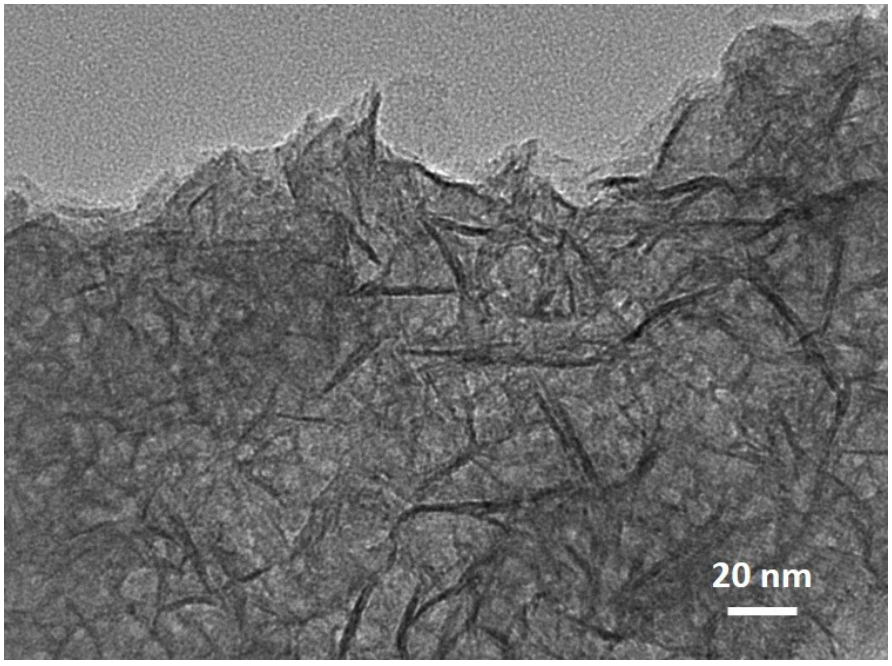

Fig. S3. Low-magnification TEM image of a piece of RT-Fe@Ni(OH)$_2$ scraped from the electrode.

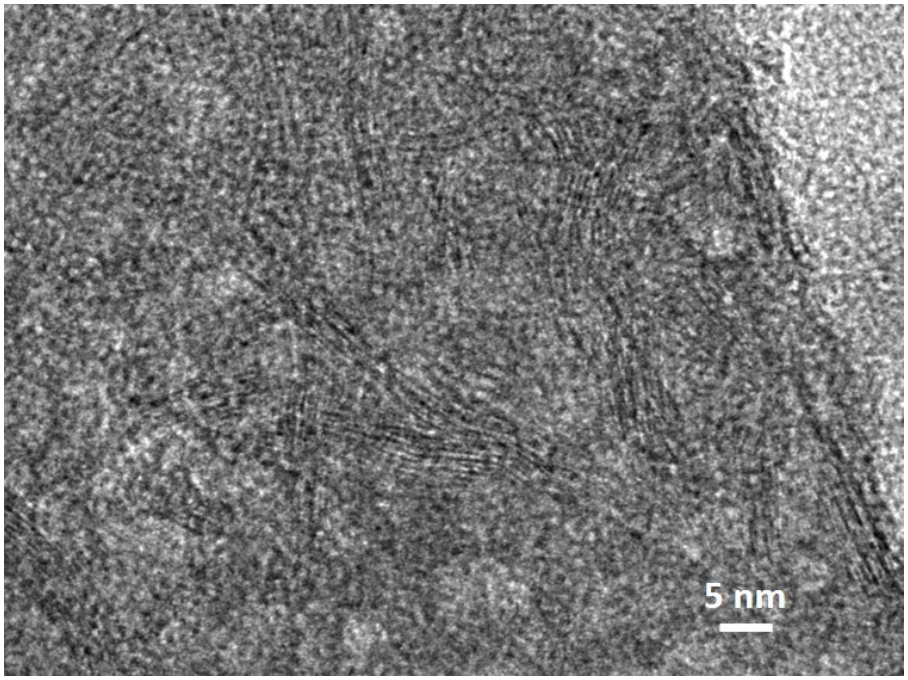

Fig. S4. HRTEM image of a piece of RT-Fe@Ni(OH)$_2$ scraped from the electrode.

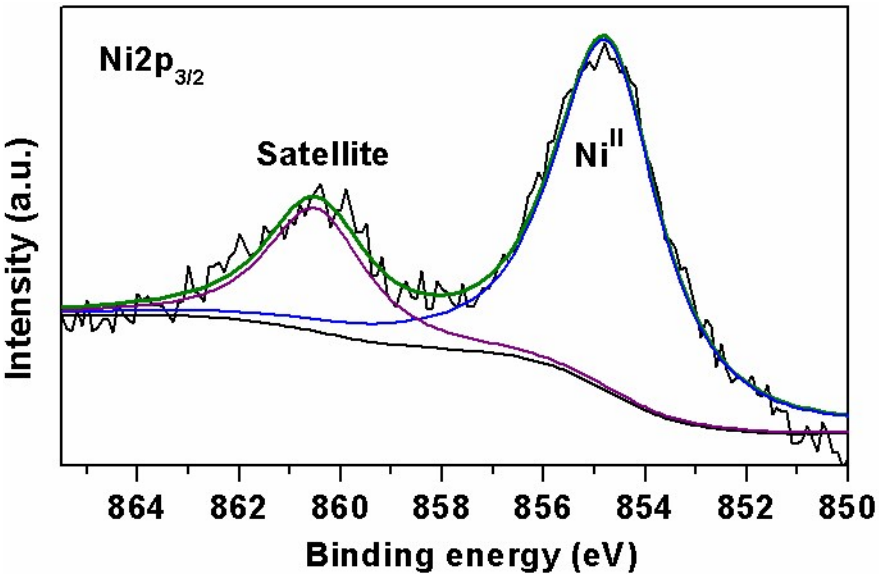

Fig. S5. XPS $Ni2p_{3/2}$ of the RT-$Ni(OH)_2$ electrode that was fabricated using similar procedure as that of the RT-Fe@$Ni(OH)_2$ electrode but without $FeCl_3$ in the etching solution.

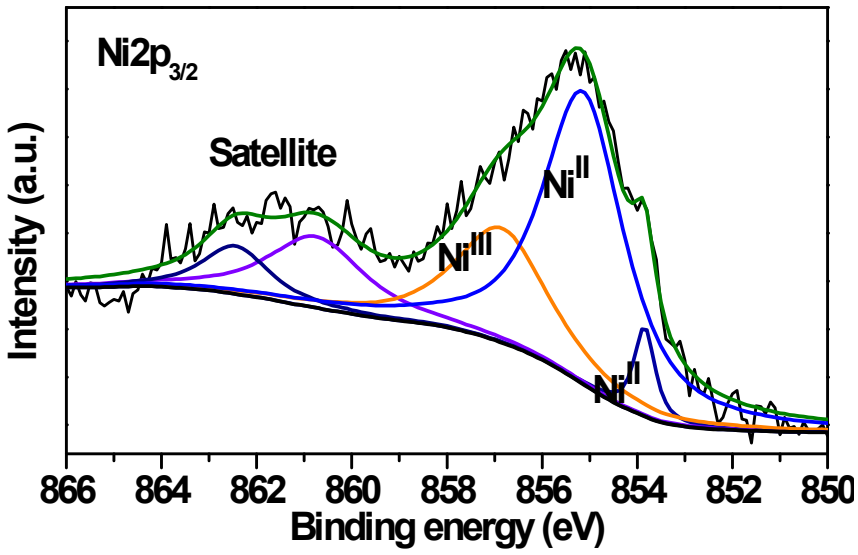

Fig. S6. XPS $Ni2p_{3/2}$ of the RT-$Ni(OH)_2$ electrode.

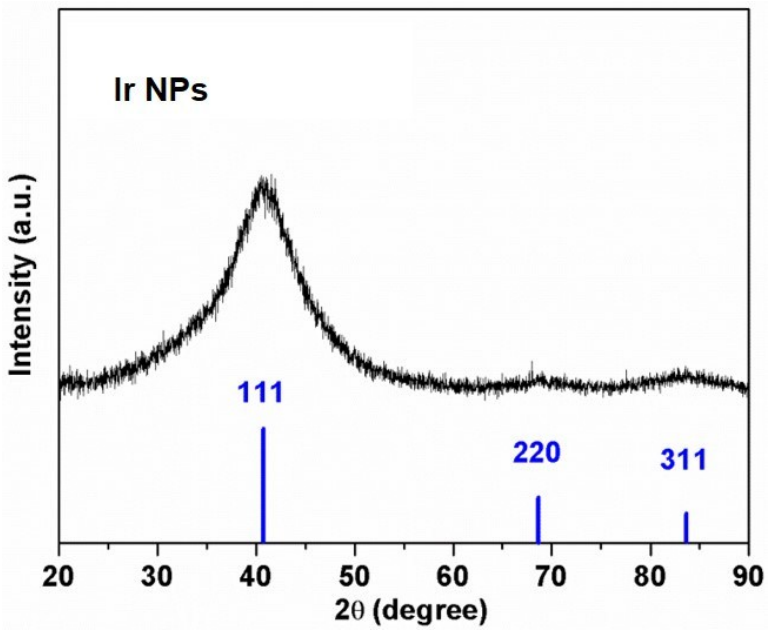

Fig. S7. XRD pattern of Ir nanoparticles (Ir NPs) used in this work.

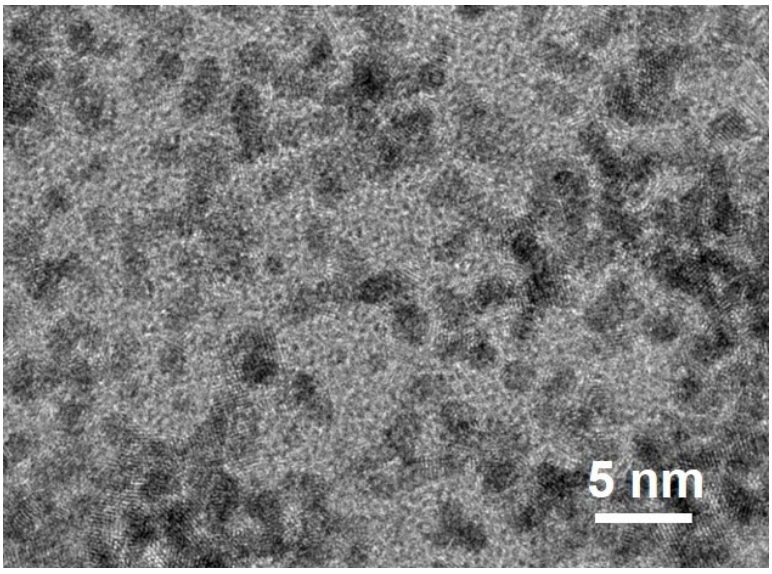

Fig. S8. TEM image of the Ir NPs used in this work.

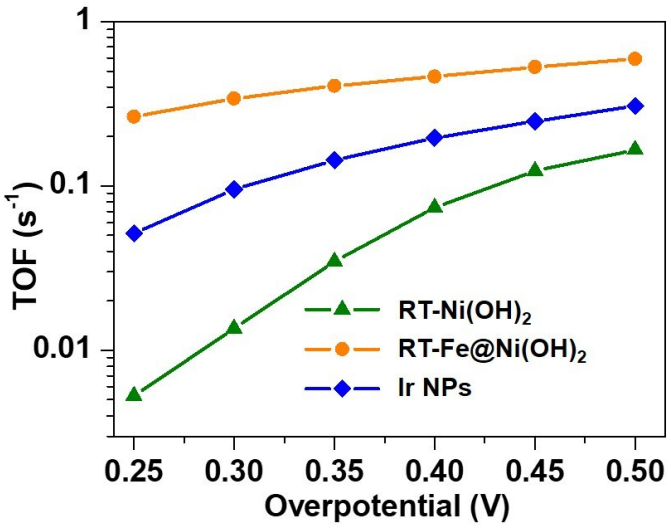

Fig. S9. Turnover frequencies (TOFs) values of the electrodes at different overpotentials.

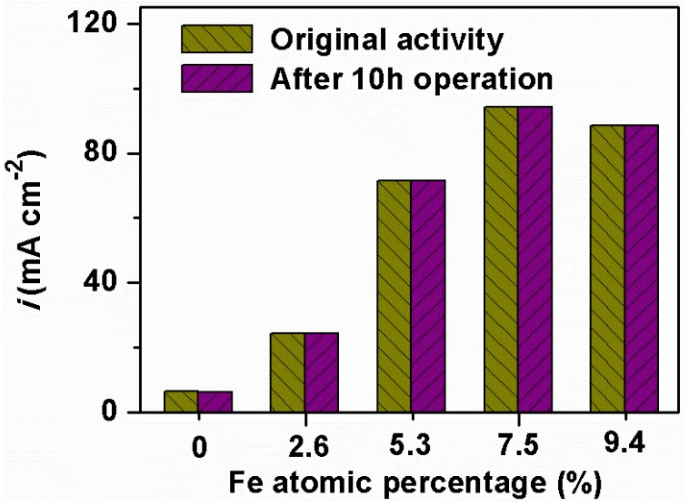

Fig. S10. Effect of Fe contents of the RT-Fe@Ni(OH)$_2$ electrodes on the OER catalytic activity and stability was studied. Testing conditions: an overpotential of 0.320 V and electrolyte of 1 M KOH.

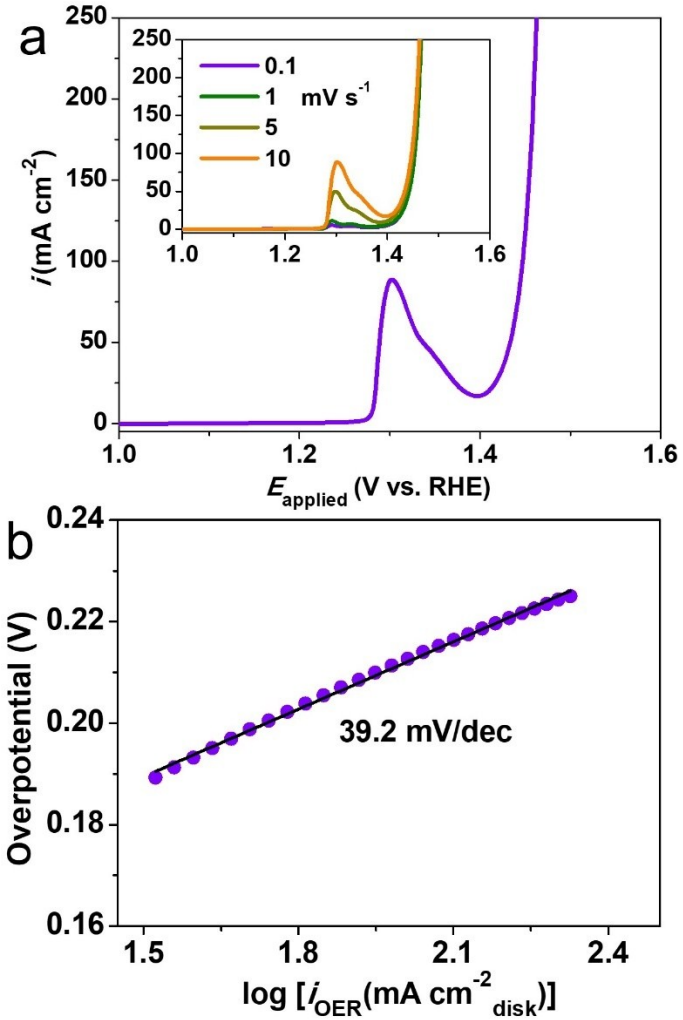

Fig. S11. OER catalytic activity of the RT-Fe@Ni(OH)$_2$ electrode in 30 wt. % KOH. (a) Polarization curve at a scan rate of 10 mV s^{-1}. The inset is polarization curves of the electrode at scan rates ranging from 0.1 to 10 mV s^{-1}. (b) Tafel plot obtained from the polarization curve at 10 mV s^{-1}.

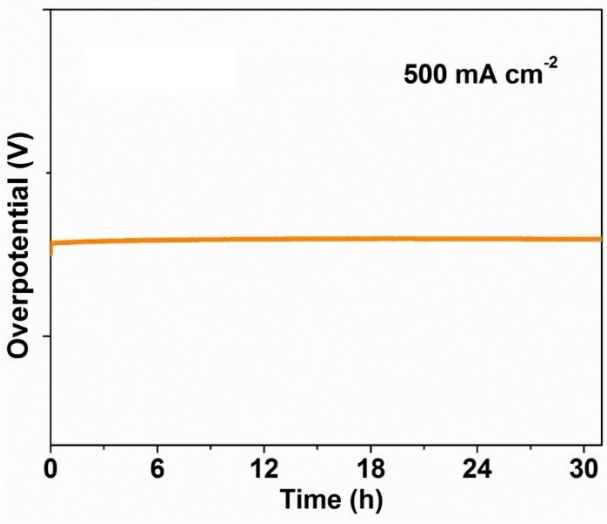

Fig. S12. OER stability of the RT-Fe@Ni(OH)$_2$ electrode in concentrated KOH (30 wt. %).

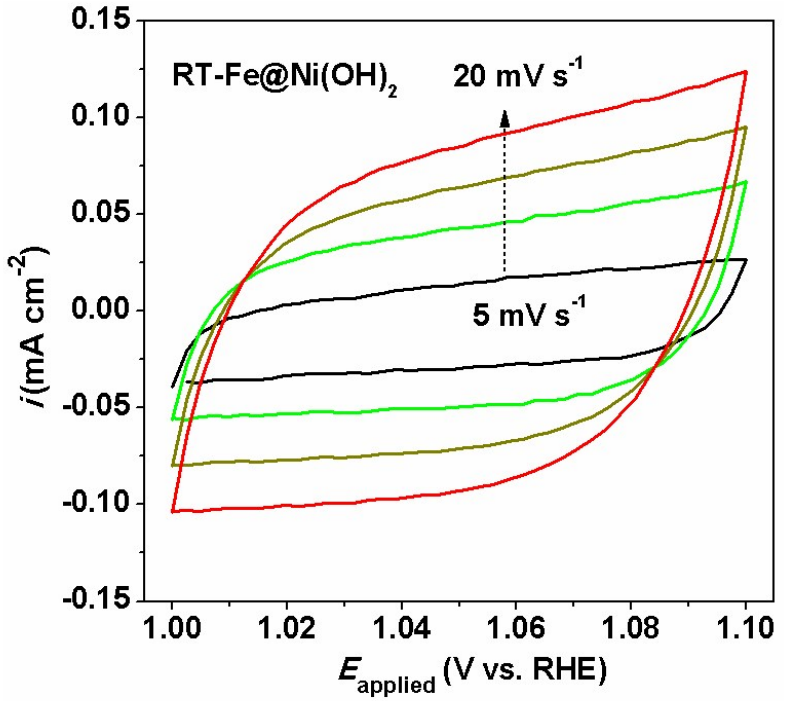

Fig. S13. CV curves of the RT-Fe@$Ni(OH)_2$ electrode with a narrow potential window at different scan rates.

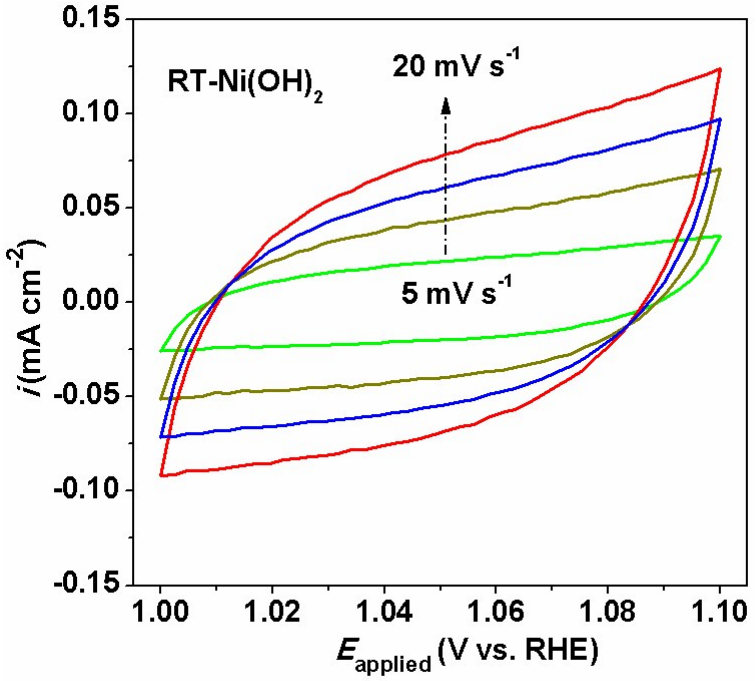

Fig. S14. CV curves of the RT-$Ni(OH)_2$ electrode with a narrow potential window of at different scan rates.

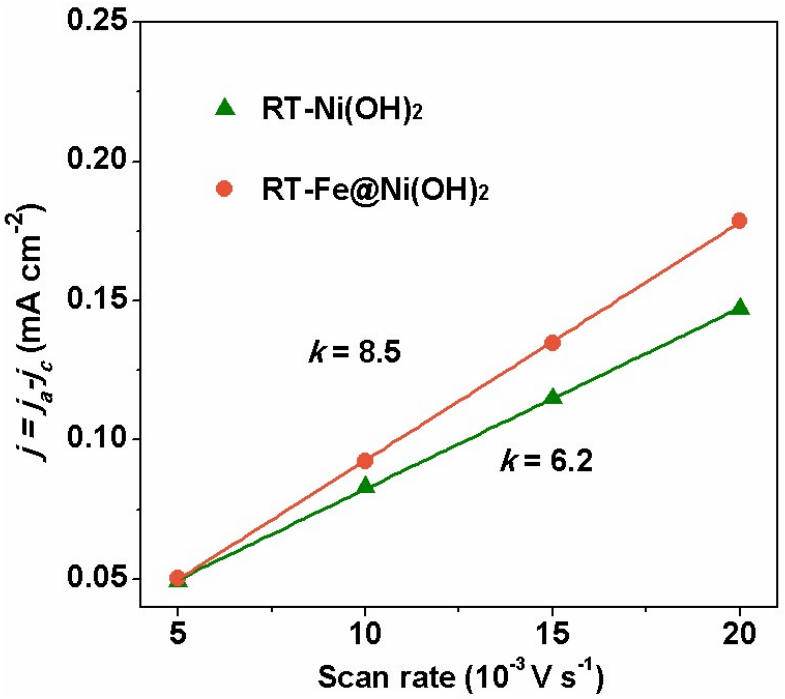

Fig. S15. Electrochemical active surface area (*ECSA*) was estimated from their electrochemical double-layer capacitance (C_{dl}) that was obtained from plots of charging current density differences against scan rates, where j_a and j_c stand for anodic and cathodic capacitive currents, respectively.

Electrochemical active surface area (*ECSA*) that is related to the active site density is an important parameter to evaluate an electrode. *ECSA* was estimated from the electrochemical double-layer capacitance (C_{dl}) that was measured in a narrow potential window to eliminate pseudocapacitance from faradic redox reactions (Fig. S13, S14). The linear slope of capacitive current ($j = j_a - j_c$) versus scan rate that is equivalent to twice of the C_{dl} was used to represent the *ECSA*. Effect of *ECSA* on OER performance of the RT-Fe@Ni(OH)$_2$ electrode was studied with the RT-Ni(OH)$_2$ electrode as comparison. *ECSA* of the RT-Fe@Ni(OH)$_2$ electrode was around 1.4-folds of that of the RT-Ni(OH)$_2$ electrode (Fig. S15), making the RT-Fe@Ni(OH)$_2$ electrode favorable in providing more active sites.

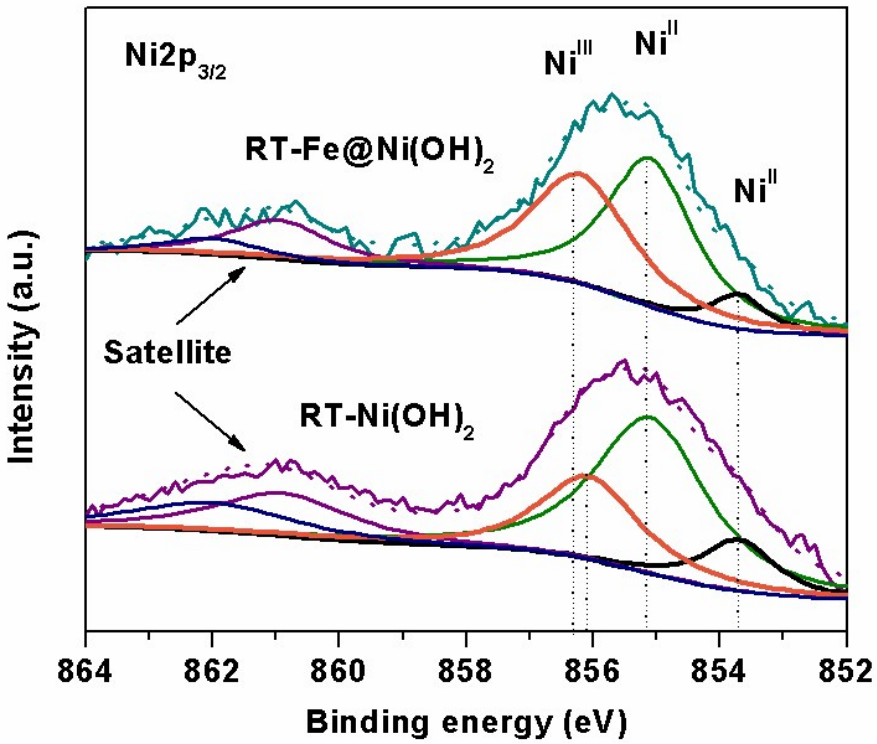

Fig. S16. XPS $Ni2p_{3/2}$ of the RT-Fe@$Ni(OH)_2$ and RT-$Ni(OH)_2$ electrode, indicating a positive binding energy shift for the RT-Fe@$Ni(OH)_2$ in comparison with the RT-$Ni(OH)_2$.